A Study of Scattering From an Object Below a Rough Surface

Joel T. Johnson, *Senior Member, IEEE,* and Robert J. Burkholder, *Senior Member, IEEE*

***Abstract*—A numerical model is applied in a Monte Carlo study of scattering from a three dimensional penetrable object below a lossy dielectric rough interface. Both time and frequency domain results are investigated to illustrate the relative importance of coherent and incoherent scattering effects in the sample problem considered. Results show that introducing a reduced transmission coefficient is reasonable for object coherent scattering predictions in this example, and that incoherent object/surface interaction effects approximately follow a simple scaling behavior as surface roughness is increased.**

***Index Terms*—Electromagnetic scattering, ground penetrating radar, radar cross section, rough surface scattering.**

I. Introduction

THE PREDICTION of scattering from an object located beneath a rough interface is a subject of recent interest, particularly due to applications in the detection of subsurface objects with radar systems. Although some approximate analytical models have been derived in the small roughness limit [1], [2], the complexity of the problem has limited the development of more general approximations. Recent works have explored numerical solutions [3]–[12], but have concentrated primarily on two dimensional scattering problems to reduce computational complexity (some three dimensional models have been presented in [8]–[12]). Results from these studies have been presented in terms of signal processing algorithm performances [3]–[5], [9], or in terms of statistics of scattered fields near the rough surface [10], [11]. However, the behaviors of coherent and incoherent backscattered fields in the far-field with three-dimensional geometries have not been a focus of previous work.

In this paper, a numerical study of scattering from a three dimensional penetrable object located below a lossy dielectric rough interface is performed to address this issue. A generalized example problem is considered to provide an illustration of some of the coherent and incoherent scattering effects which can occur, and to investigate the performance of some simple approximations for these quantities. A Monte Carlo simulation is used to obtain scattered field statistics as a function of frequency from 2–5 GHz, and results are illustrated in both the frequency and time domains to clarify the scattering physics. Results show that simple reduced transmission coefficient model [13] can remain reasonable for prediction of object coherent scattered fields. An examination of incoherent object scattered fields shows that object/surface interaction effects can make significant contributions to received object cross sections, and that a simple scaling law can provide a reasonable estimate as surface roughness is increased.

The next section briefly reviews the numerical model employed in the study, and Section III describes the particular problem for which simulations are performed. Computational issues are discussed in Section IV, and results are presented in Section V.

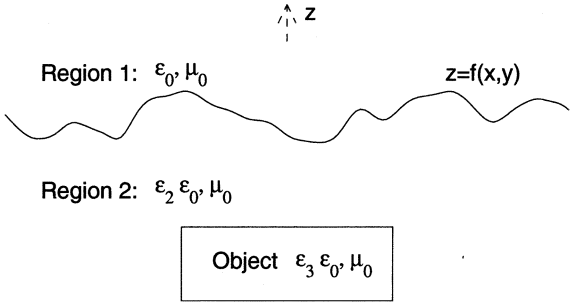

Fig. 1. Geometry of problem.

II. Numerical Model

Fig. 1 illustrates the basic geometry considered in this paper: a dielectric object with relative complex permittivity ϵ_3 is located below a rough interface $z = f(x, y)$ (of finite horizontal area as described below) between free space and a dielectric medium with relative complex permittivity ϵ_2. The numerical model applied to solve this problem is an iterative method of moments solution for single-frequency-induced volumetric currents in the dielectric object and induced electric and magnetic surface currents on the rough interface. The matrix equation formulated includes surface to surface, surface to object, object to surface, and object to object coupling, and is solved using a preconditioned Bi-CGSTAB algorithm [14]. The model is described in detail in [12], where an example of scattering from an object located below a rough interface is provided; it has also been applied in a study of scattering from an object above a rough

Manuscript received December 20, 2002; revised May 16, 2003. This work was supported in part by the National Science Foundation under Project ECS-9701678, in part by the Office of Naval Research under Contracts N00014-97-1-0541, N00014-00-1-0399, and N00014-02-1-0857, and by a grant from Duke University as part of the Office of the Secretary of Defense Multidisciplinary Research Program of the University Research Initiative (OSD MURI) on Humanitarian Demining. Use of the IBM Netfinity Linux Supercluster system at the Maui High Performance Computing Center is acknowledged, supported by the Air Force Research Laboratory, Air Force Materiel Command under Cooperative Agreement F29601-93-2-0001. Opinions, interpretations, conclusions, and recommendations are those of the authors and are not necessarily endorsed by the U.S. Air Force, Air Force Research Laboratory, or the U.S. Government.

The authors are with the Department of Electrical Engineering and ElectroScience Laboratory, The Ohio State University, Columbus, OH 43210 USA (e-mail: johnson@ee.eng.ohio-state.edu).

Digital Object Identifier 10.1109/TGRS.2003.815670

interface [15]. The model is limited by current computing performance to surface geometries which are of moderate size in terms of the electromagnetic wavelength (up to approximately $64\lambda \times 64\lambda$ profile results are reasonable at present) and of moderate roughness compared to λ. Object sizes must also remain moderate in terms of the electromagnetic wavelength.

The rough surface profiles used in the study are realizations of a Gaussian random process and for simplicity are chosen to have an isotropic Gaussian correlation function. The resulting surface statistics are described completely by the surface rms height h and correlation length l. Due to the statistical nature of this problem, scattered field results obtained from an ensemble of surface realizations are considered. While a large number of realizations is desirable for more accurate estimates of scattered field statistics, computational issues described in Section IV limit the current study to a maximum of 40 realizations. Convergence tests with the obtained data show that average cross sections estimates should be accurate to within approximately 3 dB. Both coherent (i.e., cross sections computed from the average field in the Monte Carlo simulation) and incoherent (i.e., cross sections computed from the average power minus the coherent power in the Monte Carlo simulation) are presented. Coherent cross sections provide an estimate of the average scattering behavior while incoherent cross sections provide information regarding the level of variation to be expected for differing rough surface profiles; these statistics can also be used in designing signal processing algorithms for removal of clutter contributions [4]. Although in many applications such averaged results would not be available in a given measurement, the coherent and incoherent fields to be presented comprise a basic second order statistical description of scattering in a combined object/surface problem.

Because the rough interface modeled in the simulation is of finite size, a "tapered wave" incident field is used to avoid surface edge scattering effects. Incidence angles of 0° and 45° from normal incidence are considered in this paper, and the respective tapered wave formulations are discussed in [15]. The tapered waves used in the study are chosen so that the object is well within the projected 3-dB "spot size" of the incident field while approximately 60-dB incident field attenuation is obtained at surface edges. Tests of tapered wave influence in the flat surface limit were performed through comparison with a plane wave incidence halfspace Green's function numerical solution [16]. Results of the comparison show only slight differences (within 1.5 dB) between tapered wave and plane wave radar cross sections obtained from object and object/surface interaction effects.

Due to the presence of both object and distributed source (the rough surface) scatterers, total radar cross sections obtained are dependent on the rough surface area illuminated by the incident tapered wave. For example, in the limit of a very large spot size incident field, rough surface scattering effects become more likely to dominate object scattering effects due to the larger surface area illuminated. To reduce this dependency on the incident field used, scattered fields in the study are calculated both for the combined object/rough surface problem and the rough surface only problem, and subtracted to yield "object minus no-object" fields. Coherent and incoherent cross sections obtained from these difference fields then contain only object and object/surface interaction scattering contributions which should be insensitive to the incident field used if the spot size contains the object and regions of the surface which contribute to object/surface interaction effects. Tests with larger tapered wave spot sizes confirmed that difference field cross sections showed only minor variations. Note that the object/surface interaction effects defined here include both the "direct path" interaction of a transmission through the rough surface, scattering from the object, and transmission through the rough surface back to free space, as well as higher order object/surface interactions. Surface-only incoherent cross sections will also be illustrated and compared with results from the first two terms of the small slope approximation (SSA) [17], but again remain dependent on the area illuminated.

Consideration of the primary scattering effects of this problem suggests that coherent backscattered difference fields should resemble those obtained for an object below a flat surface in the small roughness limit, and should vanish in the large roughness limit. A simple model can be developed for this process if it is assumed that the "direct path" dominates scattered fields; the basis of this model is similar to the "four-path" model of scattering from an object above a rough interface [18], but only a single path is involved for a subsurface object. The "direct path" estimate of coherent object scattered fields is obtained by computing backscattering from the subsurface object in the absence of the interface and Region 1. The incident field in this computation is the transmitted field associated with the plane wave incident from Region 1, but multiplied by a reduced transmission coefficient T_{eff} that depends on surface RMS height [13]

$$T_{\text{eff}} = T_{\text{flat}} \exp\left(-\{(k_{tz} - k_{iz})h\}^2/2\right). \tag{1}$$

Here, k_{iz} is the z component of the incident field propagation vector in Region 1, while k_{tz} is the z component of the transmitted field propagation vector. T_{flat} represents the standard Fresnel transmission coefficient at a flat interface, and h is the surface rms height. The resulting scattered fields from the "object-only" computation are again multiplied with the reduced transmission coefficient (at an angle corresponding to the direction of scattered field propagation) to model transmission from Region 2 to 1, and attenuated by path loss from the object to the interface in the case of a lossy Region 2. A refraction factor is also included to account for spherical wave refraction upon transmission from Region 2 to 1. An approximate model using this procedure for a large object below a flat interface is described in detail in [19].

Total incoherent scattered fields should be caused both by direct surface backscattering (not included in the difference fields) and by object/surface interaction effects. The "direct path" model suggests that the latter are likely to be dominated by roughness induced amplitude and phase distortions of the field incident on and scattered from the target upon transmission through the interface. However, since incoherent transmission through and scattering from the rough surface is distributed through a range of angles, incoherent object/surface interaction effects can be very complex and difficult to describe completely. Examination of time domain results in Section V

will provide some limited indications as to the most important contributions in the example considered.

A simple heuristic scaling law for incoherent backscattering contributions can be developed based on the reduced transmission coefficient behavior if it is assumed that incoherent object/surface backscattering at a given angle is completely produced by the reduction in "direct path" object coherent backscattered power at the same angle. To derive this relationship, begin by writing the "direct path" average backscattered field in the flat surface case as

$$\overline{E}_{\text{flat}} = T_{\text{flat}}^2 \overline{Q} \tag{2}$$

where $\overline{Q}$ models scattering effects that are independent of the surface profile. In the rough surface case

$$\overline{E}_{\text{rough}} = T_{\text{eff}}^2 \overline{Q}. \tag{3}$$

The difference in coherent powers $P_{\text{flat}} - P_{\text{rough}}$ is then proportional to

$$\left|T_{\text{flat}}^2\right|^2 - \left|T_{\text{eff}}^2\right|^2. \tag{4}$$

If we assume that incoherent backscattering is generated by this change in powers, then incoherent backscattering is proportional to

$$F(h) = 1 - \exp\left(-2\,\text{Re}\{(k_{tz} - k_{iz})h\}^2\right) \tag{5}$$

from (1). A prediction of incoherent backscattered power from a surface with rms height h_1, $I(h_1)$, based on knowledge of incoherent backscattered power from a surface with rms height h_2, $I(h_2)$, then follows

$$I(h_1) = I(h_2)\, F(h_1)/F(h_2). \tag{6}$$

Note a saturation of incoherent power is predicted by the scaling law as roughness becomes very large. The success of this scaling law will be evaluated in Section V for the example considered. Of course, this is a very heuristic approximation, but the absence of simple methods for incoherent scattering predictions makes investigation of this scaling law worthwhile.

III. Example Problem

A dielectric rectangular box with dimensions 7.62 cm × 7.62 cm × 2.54 cm (thickness) and relative permittivity $\epsilon_3 = 3 + i0.03$ is used as the object in this study. The center of the box is located 8.89 cm below a rough interface between free space and a medium with relative permittivity $\epsilon_2 = 5 + i1.25$. Scattering for this geometry is to be determined for a field incident at either 0° or 45° from normal incidence at multiple frequencies from 2–5 GHz. A rough surface correlation length of 3.58 cm and surface rms heights of 3.58 mm or 1 cm are used, so that the surfaces range from slightly rough at the lowest frequency ($kh = 0.15$ or 0.42, respectively, where k is the electromagnetic wavenumber) to slightly to moderately rough at the highest frequency ($kh = 0.375$ or 1.05, respectively). However, rms slopes for these surfaces are approximately 8° and 22°, respectively, making the larger height surface exceed the limitations of standard perturbation theory [20]. The problem considered could model a nonmetallic antipersonnel landmine located below a rough soil interface. Note the problem also scales with frequency, so result implications are not directly limited to the geometrical lengths above.

Time domain scattered fields are obtained from frequency swept data through a fast Fourier transform (FFT) operation preceded by multiplication with a third order Kaiser–Bessel window to reduce sidelobe levels. Time zero is defined to correspond to the center of the mean level of the rough surface ($z = 0$) in Fig. 1, so that object scattering returns occur at later times. A calculation of expected time delays shows object scattering contributions at approximate times of 1.14 and 0.91 ns for 0° and 45° incidence, respectively. Surface-only backscattering returns are centered at time zero and are spread in time from approximately −0.7–0.7 ns at 45° incidence (calculated from the 3-dB tapered wave spot size). This time spreading of surface clutter at oblique observation angles and its effects on detection of objects has been previously described in [21]. Time domain field statistics are calculated in terms of the mean and standard deviation of the field envelope as a function of time to clarify the time locations of various coherent and incoherent scattering effects. Of course, rough surface incoherent scattered fields should show no particular time location, but object/surface incoherent interaction effects do contain some time information which can help to indicate the important scattering mechanisms.

IV. Computational Issues

A 1.281 m × 1.281 m surface size is used which ranges from 8.5–21.35 free space wavelengths side dimension as the frequency varies from 2–5 GHz. The tapered wave 3-dB spot diameter with parameter $g = 5.333$ [12] is then 28.3 cm so that the object is well within the tapered wave illumination pattern. The interface is sampled into 256 × 256 points, producing a sampling rate of 5.36 points per wavelength in the dielectric medium at the highest frequency; tests with 512 × 512 points in the flat surface limit showed negligible cross section variations. While a smaller number of surface points could be used for the lower frequencies, a constant number of points sampling the rough interface as frequency is varied was chosen for convenience. The resulting number of field unknowns on the interface is 262 144. A "strong" bandwidth of 15 points and one canonical grid series term were used in rough surface matrix elements, as described in [12]; single realization tests confirmed that these parameters should provide accurate results.

The object is sampled on a 32 × 32 × 8 point grid with step size 3.175 mm (ranging from approximately 1/27 to 1/11 of the wavelength in the object as frequency varies), resulting in a total number of 13 824 object unknowns. The combined problem thus contains approximately 276 000 unknowns. While this large number of unknowns would be prohibitive for many integral equation based methods, the efficient algorithm applied (based on the order $N \log N$ "canonical grid" and "discrete dipole approximation" methods for surface-to-surface and target-to-target coupling, respectively [12]) makes the current study possible.

TABLE I
MONTE CARLO SIMULATION PARAMETERS: FREQUENCY STEP IS 200 MHz IN ALL CASES

h (mm)	Inc. angle (degrees)	Polarization	F_{min} (GHz)	F_{max} (GHz)	Number of real.
3.58	0	HH	2.2	5.0	20
3.58	45	HH	2.0	5.0	20
3.58	45	VV	2.0	5.0	20
10.00	0	HH	2.2	5.0	20
10.00	45	HH	2.0	5.0	40
10.00	45	VV	2.0	5.0	40

Although the problem considered can be solved on a PC level platform for a single realization, total computing times for the multiple cases considered in this paper were further reduced through use of IBM parallel computing resources at the Maui High Performance Computing Center (www.mhpcc.edu.). Since results as a function of frequency for multiple realizations were of interest, single-frequency/single-realization calculations were performed on individual nodes of the parallel computer (comparable to PC platforms) to obtain up to 40 realizations with 15 or 16 frequencies between 2 and 5 GHz. Monte Carlo simulation parameters for each of the cases illustrated in the next section are provided in Table I. Single-frequency computing times on a single node ranged from approximately six to fourteen hours depending on frequency, incidence angle, and surface statistics; further studies of method parameter choices and alternate iterative algorithms [12] would be likely to allow reduction of these computing times. On average, the Bi-CGSTAB iterative solver converged to a residual error less than 0.1% (the stopping tolerance used in the simulations) within four iterations. Direct path approximate model contributions were calculated using an object in Region 2 DDA code [12] with the same grid as in the combined surface/object code, and synthesized following the procedure described previously. Direct path approximate model computations of the coherent field at a single frequency required only 5 s of CPU time, emphasizing the computational advantage of this approximate method if its accuracy can be demonstrated to be reasonable.

V. RESULTS

A. Frequency Domain

Fig. 2 plots average coherent [Fig. 2(a)] and incoherent [Fig. 2(b)] object minus no-object backscattered copolarized radar cross sections versus frequency for 0° observation and for both the rms height 3.58- and 1-cm cases. Also included are the corresponding cross sections for the object below a flat surface, as well as predictions for coherent cross sections using the direct path approximate model. Coherent cross sections for the 3.58-mm rms height surface are very similar to those obtained with the object below a flat surface, while those for the rougher surface have significantly reduced amplitudes. The direct path approximate model is found to perform reasonably well for this case, indicating that its approximations remain appropriate for this example. The success of the direct path model indicates that object-surface interaction terms beyond the direct path mechanism are small for normal incidence in this problem.

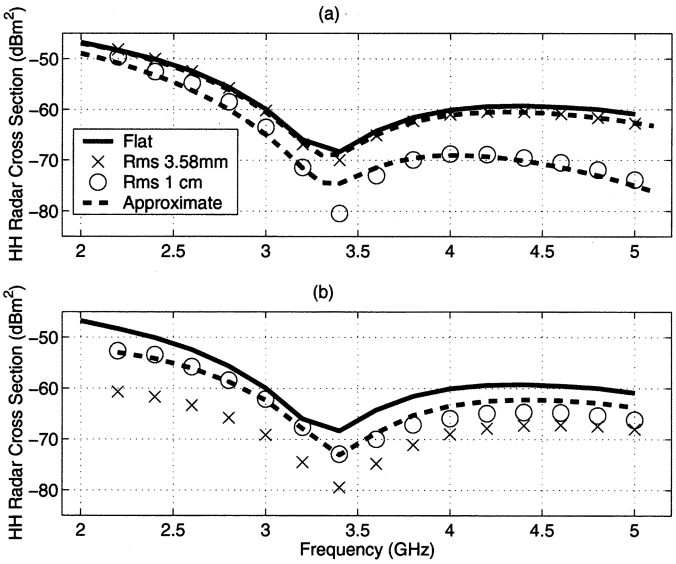

Fig. 2. Average object minus no-object backscattered radar cross sections versus frequency for 0° incidence. (a) Coherent. (b) Incoherent.

Incoherent object/surface interaction cross sections in Fig. 2(b) are found to show a behavior versus frequency similar to that of average fields for the object below a flat interface. As expected, results for the more rough surface are larger than those with the smaller roughness. For the smaller rms height surface, incoherent scattering contributions remain significantly smaller than coherent returns, while incoherent scattering is more important compared to coherent scattering for the rougher surfaces. The latter case demonstrates that object/rough surface interaction effects can make important contributions to total object scattering so that object returns below differing rough surface profiles can vary significantly. The approximate curve indicated in Fig. 2(b) applies to the larger roughness case, and is generated by multiplying smaller roughness incoherent returns by the scale factor discussed in Section II. The heuristic scale factor is shown to provide a reasonable match to numerically obtained results, indicating again that higher order surface-object interactions in this example are relatively weak.

Figs. 3 and 4 illustrate coherent [Figs. 3(a) and 4(a)] and incoherent [Figs. 3(b) and 4(b)] scattering returns for 45° incidence in HH and VV polarizations, respectively. Polarization differences should be observable in this problem for oblique incidence backscattering due to polarized object scattering and due to the polarization sensitivity of rough surface scattering at oblique angles. Coherent cross sections indeed show significant

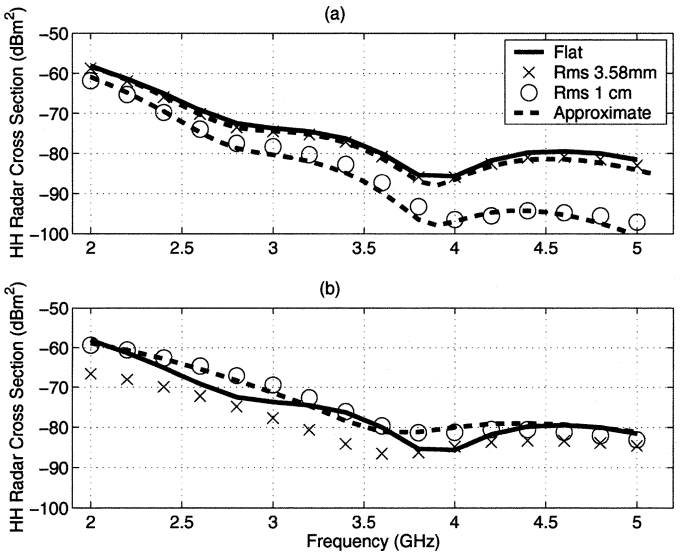

Fig. 3. Average object minus no-object backscattered radar cross sections versus frequency for 45° incidence HH. (a) Coherent. (b) Incoherent.

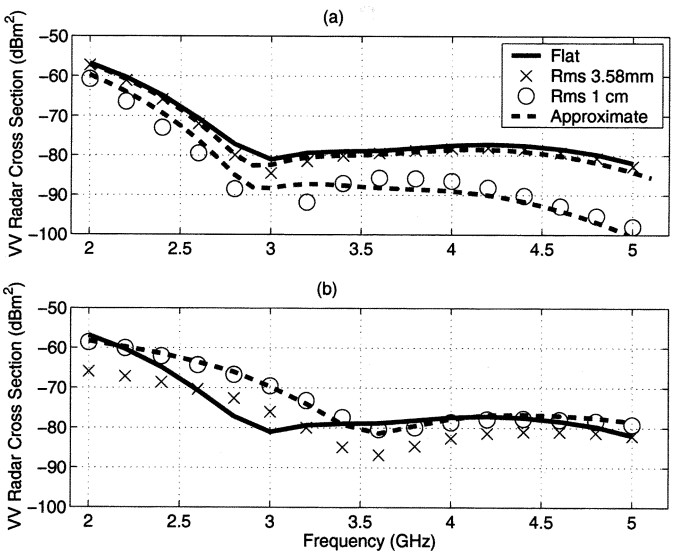

Fig. 4. Average object minus no-object backscattered radar cross sections versus frequency for 45° incidence VV. (a) Coherent. (b) Incoherent.

differences between HH and VV returns. Coherent cross sections show behaviors similar to those observed in the 0° case, and the direct path model continues to provide reasonably accurate coherent scattering predictions.

Incoherent returns in Figs. 3 and 4 show that incoherent object/surface interactions can be greater than coherent scattering even with the small height surface at some frequencies. Incoherent returns for the larger height surface are comparable to or greater than coherent returns at almost all frequencies for both HH and VV polarizations. Incoherent returns again seem to follow the basic pattern of the object return versus frequency, although larger differences are observed for oblique incidence. A possible explanation for this behavior involves the importance of "broadside" scattering for this rectangular object. For 0° incidence, this mechanism should be expected to dominate both coherent and incoherent returns, leading to the similar patterns in frequency, even if incoherent returns include some angular averaging of object returns. However, at oblique incidence, the coherent backscattering mechanism is not as dominant as at 0°, so that angular averaging plays a larger role in altering the incoherent scattering behavior versus frequency. The scaling law again provides a reasonable match to observed incoherent scattering in the larger roughness case.

A validation of rough surface-only incoherent cross sections for the specified tapered beam is presented in Fig. 5, where results at 0° [Fig. 5(a) and (b)] and 45° [Fig. 5(c) and (d)] are compared with predictions of the first two terms of the SSA. A Monte Carlo simulation using 100 surface realizations was used to obtain SSA results [22], so that the curves obtained show some residual variations due to the finite number of realizations. Numerical model results are in good general agreement with the SSA, although some differences within approximately 4 dB at the lower frequencies (where the tapered wave causes a larger degree of angular averaging) are observed. Overall the reasonable agreement obtained however validates both the numerical model and the SSA prediction for the surfaces considered. Incoherent surface only scattering at 0° generally increases with

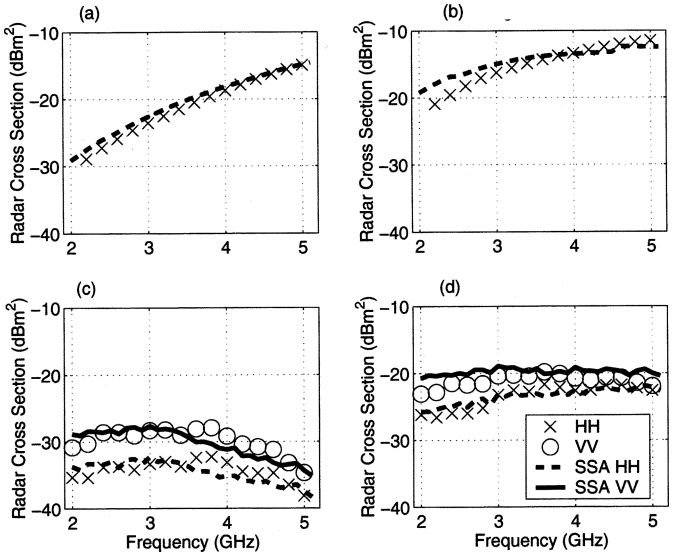

Fig. 5. Comparison of rough surface-only incoherent backscattering with small slope approximation versus frequency. (a) 0° incidence, rms height 3.58 mm. (b) 0° incidence, rms height 1 cm. (c) 45° incidence, rms height 3.58 mm. (d) 45° incidence, rms height 1 cm.

frequency, while cross sections at 45° show a decreasing trend in the small height case and only slight increases for the rougher surface. Comparisons with object/surface interaction incoherent returns in Figs. 2–4 show that surface-only incoherent scattering dominates object/surface interaction incoherent effects for the tapered beam used in all cases, due to the "low contrast" of the nonmetallic object used.

B. Time Domain

Fig. 6 presents time domain object minus no-object backscattered field envelope amplitudes (in decibels) for 0° incidence in the rms height 3.58- and rms height 1-cm cases. Both coherent [Fig. 6(a)] and "incoherent" [Fig. 6(b)] (i.e., the standard deviation of the field envelope as a function of time) returns are

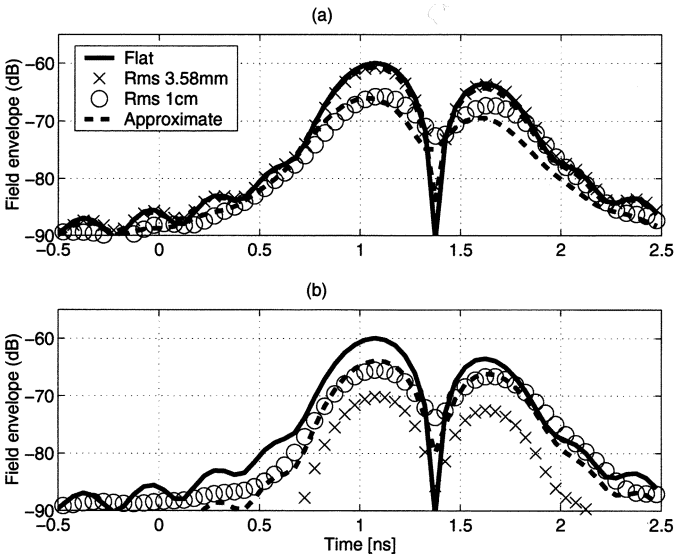

Fig. 6. Amplitude of envelope of time domain object minus no-object backscattered fields for 0° incidence. (a) Coherent. (b) Incoherent.

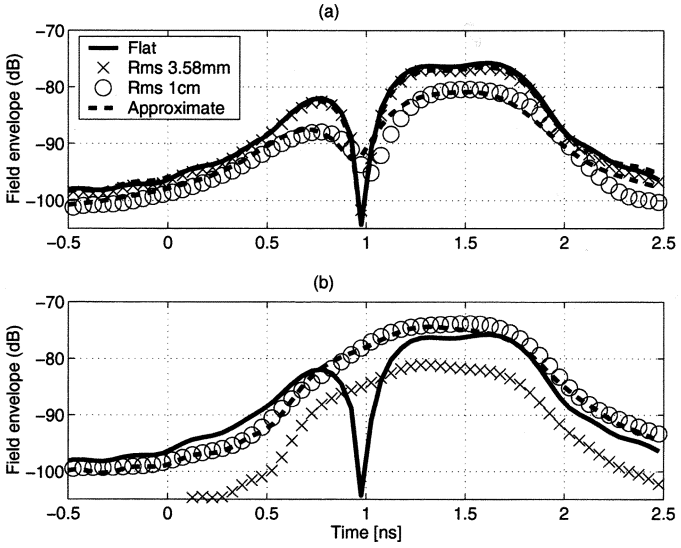

Fig. 7. Amplitude of envelope of time domain object minus no-object backscattered fields for 45° incidence HH. (a) Coherent. (b) Incoherent.

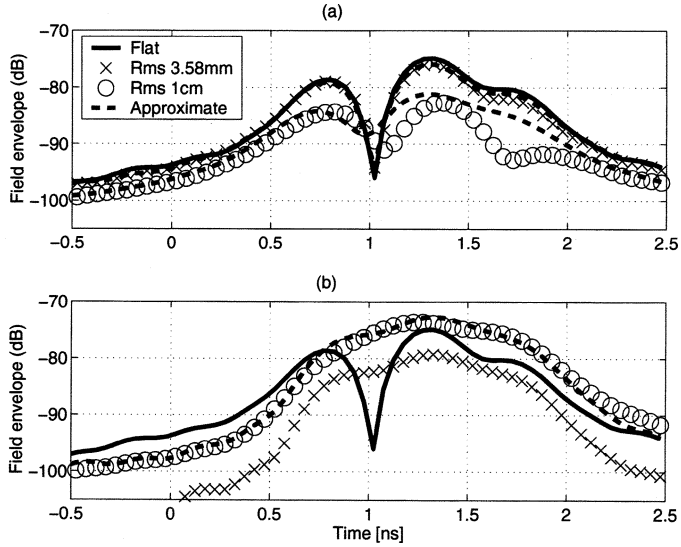

Fig. 8. Amplitude of envelope of time domain object minus no-object backscattered fields for 45° incidence VV. (a) Coherent. (b) Incoherent.

included, as well as returns with the object below a flat surface. Incoherent returns again include object/surface interaction contributions only. Coherent returns in Fig. 6 show general agreement with flat surface results for the lower rms height surface, but appreciable differences for the rougher surface. The multiple mechanisms observed in these plots can be interpreted in terms of returns from the top and bottom surfaces of the subsurface object, centered at approximate times of 1.1 and 1.5 ns, respectively. The direct path approximate model is found to continue to provide reasonable agreement in the time domain, again showing that multiple surface-object interactions are indeed small. The absence of significant returns beyond time 2 ns further confirms this statement. "Incoherent" returns in [Fig. 6(b)] again follow a similar time pattern to object results in the flat surface case, and the scaling law remains reasonably accurate. Scaling law results were generated by multiplying individual realization results by the scale factor in the frequency domain before the FFT operation. These results suggest that the primary mechanism generating incoherent returns is phase and amplitude distortion of direct path object returns caused by the rough interface; similar conclusions have been suggested in [7].

Figs. 7 and 8 illustrate coherent [Figs. 7(a) and 8(a)] and incoherent [Figs. 7(b) and 8(b)] time domain statistics at 45° incidence for HH and VV polarizations, respectively. Similar observations regarding coherent fields are obtained in this case, with only slight differences from flat surface returns observed with rms height 3.58 mm, while larger differences are observed in the rougher case as coherent fields decrease. The direct path approximation produces a similar level of agreement in the HH case, but somewhat reduced accuracy for VV. The latter case would seem to suggest that VV returns may be more influenced by multiple interactions between the object and rough surface, although the success of the direct path model in the lower rms height case indicates that these effects are not significant for flat surfaces. Incoherent returns show time domain patterns distinct from average object returns below a flat interface, unlike the 0° case, again suggesting an increased importance of angular averaging effects among other possible interactions. Incoherent returns are significant in both the low and high rms height cases, showing that time domain object returns will vary markedly with differing surface profiles. The simple scaling law continues to provide an accuracy likely to be acceptable for many applications.

For comparison, time domain surface-only backscattered field envelope amplitudes are plotted in Fig. 9 for 0° [Fig. 9(a) and (b)] and for 45° [Fig. 9(c) and (d)]. Incoherent returns for these slight to moderately rough surfaces at 0° observation show a time spread that is determined by the 3-GHz bandwidth and envelope function used, while returns at 45° are spread in time according to the tapered wave spot size. The resulting field envelopes at oblique incidence are distributed near-uniformly through the incident field illumination range, although some residual variations due to the finite number of realizations

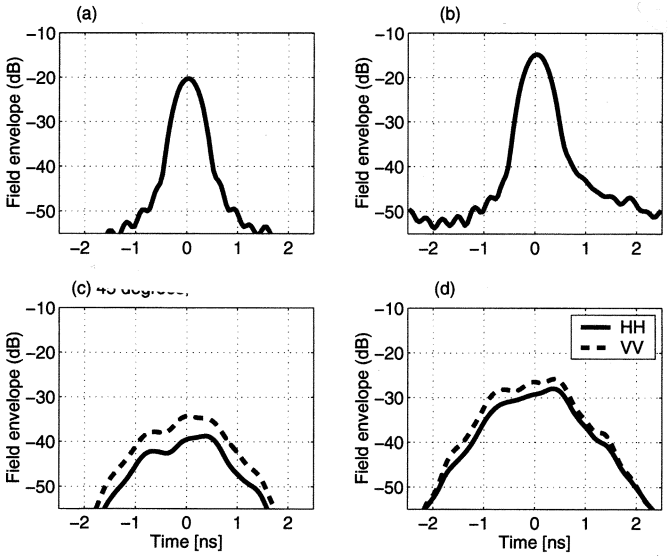

Fig. 9. Amplitude of envelope of time domain surface-only incoherent backscattered fields. (a) 0° incidence, rms height 3.58 mm. (b) 0° incidence, rms height 1 cm. (c) 45° incidence, rms height 3.58 mm. (d) 45° incidence, rms height 1 cm.

averaged remain. Note that the large surface-only returns in the 0° case occur at times prior to the smaller object-only scattering in Fig. 6, showing that object detection would be more simple for this geometry. In contrast, large surface-only returns overlap small object returns in Figs. 7 and 8, so that some form of clutter reduction or rejection would be needed in an object detection algorithm.

VI. Conclusion

The results of this study demonstrate some of the coherent and incoherent scattering effects which can occur in combined object/rough surface scattering problems. Coherent cross sections were found to resemble those for an object below a flat surface in the small roughness limit and to decrease as roughness increased. A direct path approximate model using a rough surface reduced transmission coefficient was found to match coherent cross sections well in both the frequency and time domains, although time domain accuracy was degraded for VV polarization at oblique observation. Incoherent scattered fields in both the time and frequency domains show that object/surface interaction terms can be important depending on the frequency, surface statistics, polarization, incident antenna pattern, and scattering geometry. Incoherent object/surface interaction effects observed appear consistent with a simple scale factor approximation, although complete conclusions in this regard are difficult to obtain due to the complexity of the object/surface interaction process. The success of the direct path model and of the incoherent scale factor observed in these results is of course related to the absence of strong higher order surface-object interactions in the example considered. The lossy background medium and moderate object depth in this example contribute to the absence of these higher order terms. However, computations in the flat surface case with a lossless background medium and at decreased object depths continued to be well matched by the simple direct path model, both in the time and frequency domains, even with perfectly conducting objects. These results suggest that cases with higher order object/surface interactions may be the exception rather than the rule, so that the direct path model may be applicable for many geometries. Further applications of these results and the iterative method of moments model include continued evaluation of approximate models for combined surface/object problems [1], design of improved matched filters for signal processing algorithms, and tests of object detection techniques in the presence of rough surface clutter.

References

[1] Y. Zhang, Y. E. Yang, H. Braunisch, and J. A. Kong, "Electromagnetic wave interaction of conducting object with rough surface by hybrid SPM/MOM technique," *PIER 22: Progr. Electromagn. Res.*, vol. 22, pp. 315–335, 1999.

[2] A. Ishimaru, J. D. Rockway, and Y. Kuga, "Rough surface Green's function based on the first-order modified perturbation and smoothed diagram methods," *Waves Random Media*, vol. 10, pp. 17–31, 2000.

[3] K. O'Neill, R. F. Lussky, and K. D. Paulsen, "Scattering from a metallic object embedded near the randomly rough surface of a lossy dielectric," *IEEE Trans. Geosci. Remote Sensing*, vol. 34, pp. 367–376, Mar. 1996.

[4] T. Dogaru and L. Carin, "Time-domain sensing of targets buried under a rough air-ground interface," *IEEE Trans. Antennas Propagat.*, vol. 46, pp. 360–372, Mar. 1998.

[5] A. V. der Merwe and I. J. Gupta, "A novel signal processing technique for clutter reduction in GPR measurements of small, shallow land mines," *IEEE Trans. Geosci. Remote Sensing*, vol. 38, pp. 2627–2637, Nov. 2000.

[6] A. Madrazo and M. Nieto-Vesperinas, "Scattering of light and other electromagnetic waves from a body buried beneath a highly rough random surface," *J. Opt. Soc. Amer.*, vol. 14, pp. 1859–1866, 1997.

[7] C. Rappaport and M. El-Shenawee, "Modeling GPR signal degradation from random rough ground surfaces," in *Proc. IGARSS*, 2000, pp. 3108–3110.

[8] S. Tjuatja, A. K. Fung, and J. Bredow, "Radar imaging of buried objects," in *Proc. IGARSS*, 1998, pp. 524–526.

[9] G. F. Zhang, L. Tsang, and K. Pak, "Angular correlation function and scattering coefficient of electromagnetic waves scattered by a buried object under a two-dimensional rough surface," *J. Opt. Soc. Amer.*, vol. 15, pp. 2995–3002, 1998.

[10] M. El-Shenawee and C. M. Rappaport, "Monte Carlo Simulations for clutter statistics in minefields: AP-mine-like-target buried near a dielectric object," *IEEE Trans. Geosci. Remote Sensing*, vol. 40, pp. 1416–1426, June 2002.

[11] M. El-Shenawee, C. M. Rappaport, E. L. Miller, and M. B. Silevitch, "Three-dimensional subsurface analysis of electromagnetic scattering from penetrable/PEC objects buried under rough surfaces: Use of the steepest descent fast multipole method," *IEEE Trans. Geosci. Remote Sensing*, vol. 39, pp. 1174–1182, June 2001.

[12] J. T. Johnson and R. J. Burkholder, "Coupled canonical grid/discrete dipole approach for computing scattering from objects above or below a rough interface," *IEEE Trans. Geosci. Remote Sensing*, vol. 39, pp. 1214–1220, June 2001.

[13] L. Tsang, J. A. Kong, and R. T. Shin, *Theory of Microwave Remote Sensing*. New York: Wiley, 1985.

[14] R. Barrett, M. Berry, T. F. Chan, J. Demmel, J. Donato, J. Dongarra, V. Eijkhout, R. Pozo, C. Romine, and H. van der Vorst, *Templates for the Solution of Linear Systems: Building Blocks for Iterative Methods*. Philadelphia, PA: SIAM, 1994.

[15] J. T. Johnson, "A numerical study of scattering from an object above a rough surface," *IEEE Trans. Antennas Propagat.*, vol. 40, pp. 1361–1367, Oct. 2002.

[16] E. Newman, "A user's manual for the electromagnetic surface patch code: Preliminary Version ESP5.0," ElectroScience Lab., Ohio State Univ., Columbus, OH, Unpub. Rep., 1997.

[17] A. G. Voronovich, *Wave Scattering From Rough Surfaces*. Berlin, Germany: Springer-Verlag, 1994.

[18] J. T. Johnson, "A study of the four-path model for scattering from an object above a halfspace," *Microwave Opt. Technol. Lett.*, vol. 30, pp. 130–134, 2001.

[19] J. Jenwatanavet and J. T. Johnson, "An analytical model for studies of soil modification effects on ground penetrating radar," *IEEE Trans. Antennas Propagat.*, vol. 49, pp. 923–933, June 2001.
[20] S. O. Rice, "Reflection of electromagnetic waves from slightly rough surfaces," *Commun. Pure Appl. Math*, vol. 4, pp. 361–378, 1951.
[21] J. L. Salvati, C. C. Chen, and J. T. Johnson, "Theoretical study of a surface clutter reduction algorithm," in *Proc. IGARSS*, 1998, pp. 1460–1462.
[22] S. T. McDaniel, "Acoustic and radar scattering from directional seas," *Waves Random Media*, vol. 9, no. 4, pp. 537–549, 1999.

Joel T. Johnson (S'91–M'96–SM'03) received the B.E.E. degree from the Georgia Institute of Technology, Atlanta, in 1991, and the S.M. and Ph.D. degrees from the Massachusetts Institute of Technology, Cambridge, in 1993 and 1996, respectively.

He is currently an Associate Professor in the Department of Electrical Engineering and ElectroScience Laboratory, The Ohio State University, Columbus. His research interests are in the areas of microwave remote sensing, propagation, and electromagnetic wave theory.

Dr. Johnson is a member of International Union of Radio Science (URSI) Commissions B and F, as well as a member of Tau Beta Pi, Eta Kappa Nu, and Phi Kappa Phi. He received the 1993 Best Paper Award from the IEEE Geoscience and Remote Sensing Society, was named an Office of Naval Research Young Investigator, National Science Foundation Career awardee, and PECASE Award recipient in 1997, and was recognized by the U.S. National Committee of URSI as a Booker Fellow in 2002.

Robert J. Burkholder (S'85–M'89–SM'97) received the B.S., M.S., and Ph.D. degrees in electrical engineering from The Ohio State University (OSU), Columbus, in 1984, 1985, and 1989, respectively.

He is currently a Research Scientist and Adjunct Associate Professor with the ElectroScience Laboratory, Department of Electrical Engineering, OSU. His research specialties are high-frequency asymptotic techniques and their hybrid combination with numerical techniques for solving large-scale electromagnetic radiation and scattering problems. He has contributed to the EM analysis of large cavities, such as jet inlets/exhausts and reverberation chambers, scattering from targets in the presence of rough surfaces, and the analysis of large aperture antennas radiating in realistic environments.

Dr. Burkholder is a full member of URSI Commission B and a member of the Applied Computational Electromagnetics Society.